Sting-jet windstorms over the North Atlantic: climatology and contribution to extreme wind risk

Sting-Jet Windstorms over the North Atlantic: Climatology and Contribution to Extreme Wind Risk

NEIL C. G. HART,[a] SUZANNE L. GRAY, AND PETER A. CLARK

Department of Meteorology, University of Reading, Reading, United Kingdom

(Manuscript received 7 November 2016, in final form 30 March 2017)

ABSTRACT

Extratropical cyclones with damaging winds can have large socioeconomic impacts when they make landfall. During the last decade, studies have identified a mesoscale transient jet, the sting jet, that descends from the tip of the hooked cloud head toward the top of the boundary layer in the dry intrusion region as a cause of strong surface winds, and especially gusts, in some cyclones. While many case studies have focused on the dynamics and characteristics of these jets, there have been few studies that assess the climatology of the associated cyclones and their importance for wind risk. Here the climatological characteristics of North Atlantic cyclones are determined in terms of the possibility that they had sting jets using a previously published sting-jet precursor diagnostic applied to ERA-Interim data over 32 extended winter seasons from 1979 to 2012. Of the 5447 cyclones tracked, 32% had the precursor (42% in the 22% of cyclones that developed explosively). Precursor storms have a more southerly and zonal storm track than storms without the precursor, and precursor storms tend to be more intense as defined by 850-hPa relative vorticity. This study also shows that precursor storms are the dominant cause of cyclone-related resolved strong wind events over the British Isles for 850-hPa wind speeds exceeding 30 m s^{-1}. Hence, early detection of a sting-jet storm could give advance warning of enhanced wind risk. However, over continental northwestern Europe, precursor cyclone-related windstorm events occur far less often.

1. Introduction

Damaging windstorms in the midlatitudes have long been known to be associated with extratropical cyclones. Northwestern Europe, given its location at the end of the North Atlantic storm track and high population density, is substantially exposed to windstorm risk. Since the turn of the century forecasting such storms has received much attention and the earlier empirical methods have given way to successful numerical weather prediction. Improving the resilience of societies to windstorms is aided by improved estimates of climatological windstorm risk and, if possible, how this risk might change. This paper focuses on quantifying the contribution of sting jets to windstorm risk during the recent past.

Our understanding of the processes producing windstorms has progressed through retrospective case studies of storms associated with damaging surface winds during the modern observational record. Figure 1 presents the main low-level jets known to be associated with windstorms in extratropical cyclones. Sometimes windstorms are associated with the low-level jet that forms in the warm sector of extratropical cyclones on the leading edge of the cold front (e.g., windstorm Kyrill, which swept across Europe during 17–19 January 2007; Fink et al. 2009). However, some of the strongest winds are located on the rear, equatorward flank of rapidly developing storms (Fig. 1). The Bergen school, which led development of precomputer weather forecasting methods, documented the ''poisonous tails'' of intense extratropical storms (Grønås 1995). The low-level jet forming these poisonous tails is referred to as the cool jet

Denotes content that is immediately available upon publication as open access.

[a] Current affiliation: School of Geography and the Environment, University of Oxford, Oxford, United Kingdom.

Corresponding author: Neil C. G. Hart, neil.hart@ouce.ox.ac.uk

DOI: 10.1175/JCLI-D-16-0791.1

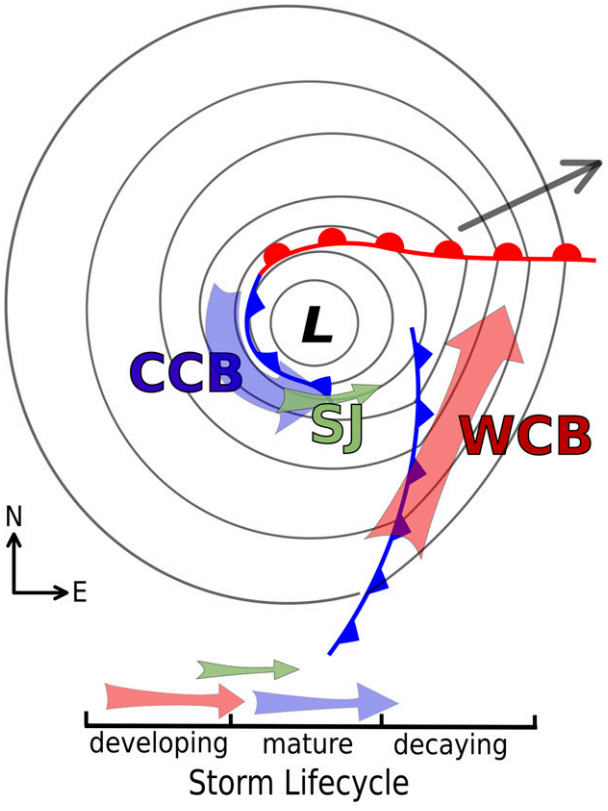

FIG. 1. Schematic of low-level jets in explosively developing extratropical cyclones. This is a composite of the jets from multiple times in the storm. Strong winds associated with the warm conveyor belt (WCB) form during storm development and those associated with the cold conveyor belt (CCB) strengthen as the storm matures. Sting jets (SJs), if forming, contribute to strongest winds during transition from WCB jet dominance to CCB jet dominance. The WCB is in the warm sector of the cyclone and has substantially warmer winds than the CCB, which is in the cool sector. The sting jet descends into the frontal fracture region where temperatures are slightly warmer than the CCB. Approximate direction of storm propagation is shown by the gray arrow.

or cold conveyor belt (Schultz 2001). Some of the most damaging windstorms happen when the cold conveyor belt winds are mixed through the boundary layer to produce extreme surface gusts (Hewson and Neu 2015).

On 16 October 1987, a poorly forecast windstorm devastated parts of northern France and southern England with wind speeds up to 55 m s^{-1} (Burt and Mansfield 1988; Shutts 1990). A case study revealed more finescale structure associated with the most severe winds (Browning 2004). A mesoscale airstream, the sting jet, was identified with the most damaging winds. This airstream arrived ahead (eastward) of the cold conveyor belt flow but behind the original cold front (Fig. 1). This region of the storm had weak boundary layer stability, favorable for the mixing of high-momentum air from the free troposphere to the surface (Clark et al. 2005). Browning (2004) discussed the occurrence of sting jets in the context of rapidly developing extratropical cyclones that develop cloud heads, warm seclusions, and bent-back warm fronts following the Shapiro–Keyser model of a cyclone life cycle (Shapiro and Keyser 1990). Clark et al. (2005) demonstrated that the sting jet was an airstream that descended from the tip of the midtroposphere cloud head into the frontal fracture region behind the cold front. The dynamics producing sting jets and associated surface gusts remains an active research area (Gray et al. 2011; Martínez-Alvarado et al. 2014; Schultz and Sienkiewicz 2013; Browning et al. 2015). With respect to windstorms, sting jets are sometimes the primary cause of extreme winds in this part of the cyclone, such as in the Great Storm of October 1987; however, in other cases they are likely to enhance strong winds already present in the cold conveyor belt. Since the power of wind increases with the cube of the wind speed, small enhancements to total wind can substantially increase windstorm severity. A conceptual model of windstorm development based on analysis of historic storms and a synthesis of extratropical cyclone literature is presented in Hewson and Neu (2015).

The mesoscale meteorology of windstorms needs to be placed into the larger-scale context of storm tracks to build a more complete quantification of windstorm risk. The climatologies of extratropical storm tracks have been studied in detail using reanalyses (e.g., Simmonds and Keay 2000; Hoskins and Hodges 2002) by applying various feature-tracking methods (e.g., Murray and Simmonds 1991; Hodges 1994). The North Atlantic storm track has been studied extensively, with much recent work focusing on the dynamics governing its position and how these are represented in model simulations of present and future climates (e.g., Zappa et al. 2013). However, climate models with horizontal grid spacing coarser than approximately 80 km and even state-of-the-art numerical models used in producing modern reanalyses have insufficient resolution to fully represent explosive cyclone development and the associated mesoscale detail needed to quantify windstorm risk (Hewson and Neu 2015; Pirret et al. 2017).

Roberts et al. (2014) detailed the 50 most extreme windstorms known to have impacted Europe. Detailed footprints of surface gusts were produced for each storm by using a limited-area numerical model with a horizontal grid spacing of 24 km to downscale ERA-Interim data. However, sting jets have horizontal scales of around 50 km (or less) and are associated with slantwise motion with a slope of typically 1/50. Thus, a horizontal grid-spacing of around 10 km or less and midtropospheric vertical grid spacing of around 200 m or less is

required to adequately resolve the flow (Clark et al. 2005).

Martínez-Alvarado et al. (2013) proposed an indirect method to assess sting-jet-associated windstorm risk by identifying environmental conditions that are precursors to the development of sting jet airstreams. This so-called "sting-jet precursor" diagnostic uses the amount of instability to moist slantwise motions in the cloud head of extratropical storms. Coarse-resolution global weather forecast and climate projection models generate this instability but are unable to release it through the slantwise-descent characteristic of sting-jet airstreams (Martínez-Alvarado et al. 2013). The study reported by Martínez-Alvarado et al. (2012) applied the precursor diagnostic to 100 extratropical cyclones in reanalysis data from 1979 to 2012 in the North Atlantic and demonstrated it to have skill in the identification of cyclones likely to have had sting jets.

The study of Martínez-Alvarado et al. (2012) was a significant step toward the assessment of the relative importance of sting-jet cyclones in the North Atlantic and, by inference, the wind risk associated with them. It was limited, however, in that it considered only 100 cyclones, was focused on the demonstration of the skill of the precursor diagnostic as a predictor for sting jets, and did not consider the wind strength of the cyclones. Many questions remain. In this study we apply the methodology of Martínez-Alvarado et al. (2012) increasing the number of cyclones studied to all North Atlantic cyclones tracked in a reanalysis dataset over 32 extended winter seasons (5447 cyclones) and address the following questions:

1) What proportion of cyclones have sting-jet precursors, and how do they compare in terms of their intensity metrics to cyclones without these precursors?
2) Do cyclones with sting-jet precursors have track and seasonal cycle characteristics distinct from cyclones without this precursor?
3) Do cyclones with sting-jet precursors exhibit higher wind risk than those without even without taking account of the sting-jet development?

Answering these questions will reveal whether the possible presence of sting jets in cyclones needs to be considered when determining windstorm risk over the North Atlantic and northwestern Europe.

The remainder of this paper is structured as follows. The data used and calculations of the sting-jet precursor and cyclone wind footprints, including the delineation into cool- and warm-sector winds, are described in section 2. Careful justification for the use of 850-hPa wind speeds as an indicator of windstorm risk is included in this section. The results section (section 3) is split into three sections to address the three questions posed above separately. Section 4 contains a summary together with interpretation of the results and their implications for windstorm risk in northwestern Europe.

2. Methods

a. Cyclone data and suitability

Extratropical cyclone tracks derived from the European Centre for Medium-Range Weather Forecasts (ECMWF) interim reanalysis (ERA-Interim, hereafter ERA-I; Dee et al. 2011) were obtained for this study. The tracks were calculated using the TRACK algorithm (Hodges 1995; Hodges et al. 2011) applied to 6-hourly 850-hPa relative vorticity ζ_{850} smoothed to spectral T42 resolution. An extended September–May winter season is used including data from September 1979 to May 2012. Cyclones that reach maximum relative vorticity $\zeta_{\max}$ within a midlatitude North Atlantic domain—45°–70°N, 80°W–40°E—are retained for further analysis here.

The model used to generate ERA-I (spectral T255 resolution, equivalent to about 80-km grid spacing) is capable of simulating the synoptic-scale winds associated with extratropical cyclones. For example, Catto et al. (2010) identified conceptual features of cyclones such as conveyor belts in composites derived from the older ECMWF reanalysis, ERA-40, and Hodges et al. (2011) found that composite cyclone diagnostics are very similar in four recent reanalyses including ERA-I. However, the model used to generate ERA-I cannot resolve mesoscale flows, such as sting jets, associated with more local wind maxima. Given this, how can reanalysis data be used to assess the wind risk posed by sting-jet cyclones? Although sting jets do not explicitly exist in the ERA-I data, we can still use the data to identify cyclones that are likely to have had sting jets, as described in the next section.

b. DSCAPE diagnosis

Gray et al. (2011) demonstrated that downdraft slantwise convective available potential energy (DSCAPE) was present in the cloud heads of three cyclones with sting jets (and not present in the cloud head of an intense cyclone that did not have a sting jet) and that release of DSCAPE occurred during the sting-jet descent. This finding is consistent with earlier studies (Browning 2005; Clark et al. 2005) that argued that the release of conditional symmetric instability (CSI) enhances the acceleration of the sting jet during descent.

Martínez-Alvarado et al. (2012) showed that DSCAPE accumulated in the cloud head of some cyclones in the ERA-I dataset. As the resolution of the model used to generate ERA-I is insufficient to resolve slantwise descents that release DSCAPE, it is likely that the accumulation is ultimately released through an alternative route. This release may occur in the convection scheme if the CSI becomes converted to conditional instability (CI) as suggested by Gray et al. (2011). The accumulation of DSCAPE can be exploited to diagnose the potential for the slantwise descent from the cloud head, and Martínez-Alvarado et al. (2012) used it to develop the sting-jet precursor diagnostic that is used, with minor modification, in this study. The 6-hourly ERA-I data used to compute DSCAPE are on pressure levels with a vertical increment of 25 hPa.

Full details of the DSCAPE-based sting-jet precursor calculation are available in Martínez-Alvarado et al. (2012), including sensitivity to the thresholds chosen, and so only the key points and modifications to the previously published method are summarized here. Calculation of DSCAPE is analogous to the calculation of downdraft convective available potential energy (DCAPE; Emanuel 1994) but calculated along constant absolute momentum surfaces instead of vertically. The momentum surfaces are defined by the vector (M, N), where $M = fx + v$ and $N = fy - u$, with f the Coriolis parameter, (x, y) the Cartesian coordinates, and (u, v) the wind velocity components. Absolute momentum surfaces are computed throughout the cloud head of tracked cyclones by considering each grid point at a given pressure level p_{top} (e.g., 400 hPa) and searching for the equivalent (M, N) value at the pressure level located below (425 hPa in this example). This procedure continues to a near-surface level (950 hPa) yielding (M, N) trajectories onto which thermodynamic variables are interpolated. Integrating along each trajectory yields DSCAPE for the grid point and level from which the trajectory is calculated:

$$\text{DSCAPE} = \int_{p_{\text{top}}}^{950\text{hPa}} R_d(T_{v,e} - T_{v,p}) d\ln p, \qquad (1)$$

where R_d is the gas constant for dry air; $T_{v,e}$ and $T_{v,p}$ are the environmental and parcel virtual temperatures, respectively; and p is pressure. The calculation is performed for p_{top} values ranging from 400 to 800 hPa inclusive (25-hPa increments), and the maximum value for the grid column is retained. To reduce processing time, (M, N) trajectories are only started from grid points with relative humidity exceeding 80%—to allow for some subgrid variability—since DSCAPE can theoretically only be released for saturated air parcels. This is a minor modification to the method in Martínez-Alvarado et al. (2012), in which this saturation threshold was applied after, instead of before, the calculation of DSCAPE.

c. *Sting-jet precursor diagnosis*

The five steps performed to identify cyclones with sting-jet precursors using the DSCAPE diagnostic are summarized as follows:

1) Match the cyclone track points derived from ζ_{850} to associated mean sea level pressure (MSLP) minima. We retain the cyclones that have a proximal association with a surface low within ±42 h of $\zeta_{\max}$. This MSLP minima is a better representation of the cyclone center than $\zeta_{\max}$, which is usually found in the strongest winds equatorward of the storm.
2) For each cyclone track point, calculate the DSCAPE within 700 km of the MSLP minima using the method detailed above.
3) Identify cases with substantial DSCAPE in the cloud head by applying the following thresholds within a 700-km radius: DSCAPE $> 200\,\text{J kg}^{-1}$, magnitude of temperature gradient $|\nabla\theta_w| > 10^{-4}\,\text{K m}^{-1}$ (where θ_w is wet bulb potential temperature), and temperature advection $\mathbf{v} \cdot \nabla\theta_w > 10^{-4}\,\text{K s}^{-1}$ (where $\mathbf{v}$ is the vector for horizontal velocity).
4) Determine contiguous volumes where these conditions are satisfied and retain those for which all points in the volume are within the cyclone sector defined as 100°–300°, where 0° is set to the axis of cyclone propagation determined as the line joining the current and next track point.
5) Classify a cyclone as having a sting-jet precursor if it has a retained contiguous DSCAPE region of at least eight model grid volumes for at least one track point.

We have used a minimum of eight model grid volumes rather than five as in Martínez-Alvarado et al. (2012) as a more conservative estimate of the importance of sting jet cyclones for wind risk. Using five model grid volumes (not shown) instead led, as expected, to more cyclones with the precursor being identified (the number of explosively developing storms with the precursor increased by 29%) and increased contribution of these storms to windstorm risk over the British Isles and continental western Europe. However, the overall conclusions presented in this paper are robust to this threshold choice. Sensitivity to the many thresholds specified in the precursor diagnostic is discussed in detail in Martínez-Alvarado et al. (2012), acknowledging the inherent arbitrary nature of such values. Nevertheless, the study found that the sting-jet precursor diagnostic had significant skill in the identification of cyclones,

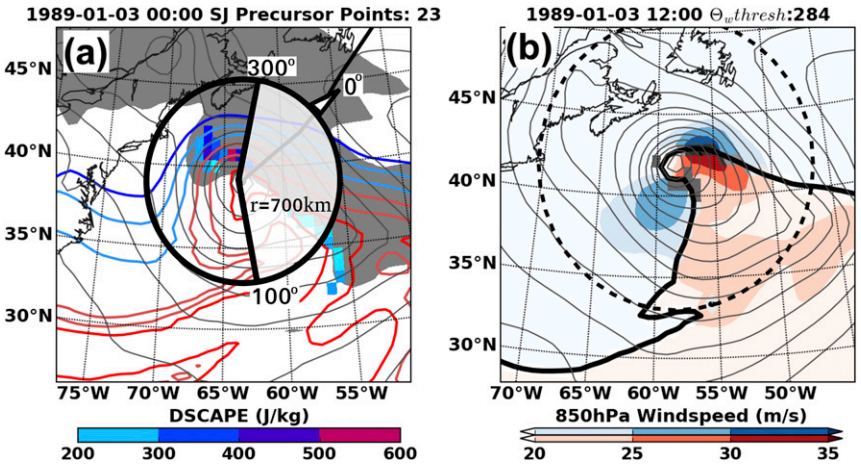

FIG. 2. Methodology example using the ERICA IOP4 storm as represented in ERA-I. (a) Sting-jet DSCAPE precursor (color shading), 850-hPa θ_w contours (colored; every 2 K starting at 277 K in blue) and MSLP (gray contours every 3 hPa) with RH > 90% in the lower midtroposphere (considered in the layer from 600 to 850 hPa) in gray shading to indicate the cloud head. Northeastward cyclone movement is indicated by system track (thick black line). To satisfy the precursor diagnostic DSCAPE values must be proximate to the cyclone center (within a circle of radius 700 km) and within the rearward-developing cloud head (clear sector in circle bounded from 100° to 300° when 0° is defined as the direction of cyclone movement). (b) Resolved wind speed (850 hPa) separated into cool- and warm-sector resolved winds (blue and red shading, respectively) by a θ_w threshold (284 K; black line). This threshold is the mean θ_w value obtained from grid points exceeding the 99th percentile of $\nabla\theta_w$ (gray shaded areas) within a 1000-km radius of the cyclone center.

which, when simulated at sting-jet resolving resolution, produced sting jets. Of 15 cyclones tested (drawn randomly from 100 intense cyclones, 7 with and 8 without a sting-jet precursor) the presence or absence of the precursor correctly predicted whether a sting jet formed in 12 cases: there were two false alarms and one missed case.

A number of caveats must be considered for the results presented here:

1) Although the precursor has skill as a predictor of the presence or absence of a sting jet in a cyclone, it cannot be assumed to be 100% accurate.
2) The precursor specifically indicates the likely presence of sting jets enhanced by or due to the release of CSI. Other mechanisms may exist that produce similar enhanced winds.
3) The strength of the precursor does not directly predict the strength of the sting jet, but it can be taken as an indicator of confidence that a sting jet would have formed.

The application of the sting-jet precursor diagnostic is illustrated in Fig. 2a for a case example, the cyclone that was the focus of intensive observing period 4 (IOP4) of the Experiment on Rapidly Intensifying Cyclones over the Atlantic (ERICA) field campaign (Neiman and Shapiro 1993; Neiman et al. 1993). The cyclone had a well-developed cloud head and has a fractured frontal zone to the south of its center at the time shown. DSCAPE values exceeding the 200 J kg^{-1} threshold are found for 13 grid volumes in the cloud head within the permitted sector (the clear sector within the circle centered on the location of the MSLP minimum). Hence, this cyclone satisfies the criteria for the sting-jet precursor diagnostic at this time and so is included in the set of cyclones that exhibit the precursor.

d. Wind risk diagnosis

It must be emphasized that the wind strength used in the following analysis is that actually developed in the ERA-I data. It does not include any direct impact of a sting jet for reasons explained above. To maintain clarity throughout, we shall use the term "resolved wind" in the following.

Wind footprints are defined for each cyclone from 6-hourly 850-hPa resolved wind speeds exceeding specified thresholds within a 1000-km radius of the cyclone MSLP centers. We have chosen to use the wind speed at 850 hPa as a realistic, if rough, estimate of the most damaging gusts possible at the surface for the following reasons.

The damage done by the winds in extratropical cyclones is primarily caused by short-period gusts, as they

contain the most energy. These may be caused by a number of mechanisms, such as deep convection or local orography, but the most general gusts are those associated with boundary layer turbulence. It is important to take gust strength into account when estimating damage; using the mean wind at, say, 10-m height is grossly misleading, especially as a cyclone makes landfall. The surface roughness causes a rapid decrease in mean wind but also a consequent considerable increase in turbulence intensity. We assume that the turbulence intensity is measured by the standard deviation of horizontal wind due to boundary layer turbulence σ_u. The gust strength depends upon the time or length scale over which the wind is averaged (or over which a gust acts to do damage)—shorter gusts with a given speed are more probable than longer ones, or, conversely, for a given averaging time, stronger gusts are less probable. To completely understand the impact of a storm one needs to understand both the gust spectrum and the impact of gusts on a given structure: a general measure is not possible. Wieringa (1973) discusses this in some detail. The result amounts to a formula of the form

$$u_{\text{gust}} = u_{10} + k_p \sigma_u , \tag{2}$$

where k_p essentially measures how "extreme" the gust is and depends upon averaging times and the shape of the gust distribution. However, a value of 3 has often been used for k_p in the general wind-loading literature. The boundary layer turbulence intensity, according to standard boundary layer scaling laws, can be written as follows (Panofsky et al. 1977):

$$\sigma_u = u_* [12 + 0.5 z_i/(-L)]^{1/3}, \tag{3}$$

where u_* is the friction velocity, z_i the boundary layer depth, and L the Obukhov length. This is essentially just a combination of the friction velocity and the convective velocity scale w_*:

$$\sigma_u = (a u_*^3 + b w_*^3)^{1/3}, \tag{4}$$

since $w_*^3 = (u_*^3/\kappa)(z_i/-L)$, where κ is von Kármán's constant and a and b are constants. This is the basis of the gust diagnostic used by Clark et al. (2005) for the sting jet in the 1987 storm, but these authors found that $k_p = 4$ reproduces observed gusts better, though gusts are still slightly underpredicted.

More traditionally, forecasters have used winds taken from higher levels, typical of near the top of the boundary layer as an indicator of gust strength, on the grounds that this is the maximum wind achievable purely by mixing. At strong wind speeds, the convective component can probably be neglected; the boundary layer is near neutral to moist mixing in the boundary layer in the sting jet. We can easily reconcile these approaches. In neutral conditions, the wind profile is

$$u(z) = \frac{u_*}{\kappa} \ln\left(\frac{z}{z_0}\right). \tag{5}$$

Hence, to determine the height z_{gust} at which the mean wind speed equals that of the surface wind gusts, consider the following:

$$\frac{u_*}{\kappa} \ln\left(\frac{z_{\text{gust}}}{z_0}\right) = u_{10} + k_p \sigma_u \tag{6}$$

$$= \frac{u_*}{\kappa} \ln\left(\frac{10}{z_0}\right) + k_p 12^{1/3} u_* \tag{7}$$

$$\Rightarrow \ln\left(\frac{z_{\text{gust}}}{10}\right) = \kappa 12^{1/3} k_p \tag{8}$$

$$\approx k_p , \tag{9}$$

where the final approximation is consistent with Wieringa (1973). So the equivalent height depends (in neutral conditions) only on the degree of extreme. If $k_p = 4$, this would give $z_{\text{gust}} = 546$ m, but more extreme damage, a value of $k_p = 5$ gives $z_{\text{gust}} = 1484$ m. It is, of course, incorrect to assume that a logarithmic profile extends to these heights, but these numbers justify the idea that the most damaging gust corresponds to winds at heights $O(1)$ km. In choosing to standardize on the wind speed at 850 hPa as an estimate of the most damaging gusts possible at the surface, we have erred on the side of "too high" to ensure no underprediction over land. The difference between 850-hPa winds and, say, 900-hPa winds is likely to be small, but winds at the 900-hPa level are likely to be affected by the boundary layer mixing in many cases, especially those with deep low pressure centers. More complex estimators for gust exist (Sheridan 2011). Most estimators related to boundary layer gusts are either based on scaling laws similar to the above or choosing a height such as the top of the boundary layer; these may have advantages but differ little in practice from our simpler approach and generally contain variables not directly available in ERA datasets. We regard it as highly desirable to use a wind-risk indicator readily available in most datasets and not strongly affected by underlying topography.

Thus, resolved 850-hPa wind risk maps are calculated showing the number of times per year that each grid point is within a wind footprint of given wind speed threshold. Resolved winds are then classified as cool- or warm-sector resolved winds through comparison of the gridpoint 850-hPa θ_w values with a value calculated as

TABLE 1. Cyclone numbers classified by type of development (explosive or nonexplosive) and presence or absence of sting-jet precursor. Percentages of total number of cyclones (5447) shown in parentheses.

	Nonexplosive	Explosive	Totals
Nonprecursor	3020 (55%)	676 (12%)	3696 (68%)
Precursor	1252 (23%)	499 (9%)	1751 (32%)
Totals	4272 (78%)	1175 (22%)	5447

indicative of the frontal boundaries in the cyclone. This classification reveals whether strong wind events are associated with the warm or cold conveyor belt jet. The frontal θ_w value is calculated as the mean θ_w value at model grid points where the gradient $\nabla\theta_w$ exceeds the 99th percentile of values for all points within 1000 km of the cyclone center. The cool and warm sectors are then simply considered as everywhere where θ_w is less or more than the frontal θ_w, respectively. Figure 2b illustrates the application of the method to distinguish cool- and warm-sector resolved winds. The cyclone example used is again from ERICA IOP4 (as for Fig. 2a), but 12 h later when the resolved winds were stronger. The gray squares mark the grid points where $\nabla\theta_w$ exceeds the 99th percentile; these are mainly found along the cold front, just south of the zone of frontal fracture. The average θ_w of these grid points is 284 K, contoured with the thick black line, and is used to define the frontal boundary between the cool and warm air. Tests showed that the 99th percentile of $\nabla\theta_w$ best captured the sharpest frontal gradients of the cyclone in the cold front. Lower percentiles tended to become dominated by the weaker frontal gradients in the warm front region resulting in computation of a temperature threshold less appropriate for delineation of the cool and warm sectors of each cyclone. Nevertheless, the sensitivity of the results (presented in Figs. 9 and 10) to this threshold was tested by producing equivalent figures but instead using the 95th and 97th percentiles. There were small changes (e.g., the proportional contributions of warm-sector resolved winds increased slightly for the lower percentiles), but these did not affect the conclusions drawn.

3. Results

a. *Prevalence of cyclones with and without sting-jet precursors*

The categorization of the tracked cyclones into explosively and nonexplosively developing and those with and without sting-jet precursors, is presented as a 2×2 contingency table in Table 1. Here explosive development is defined as occurring if the minimum MSLP deepens by more than 20 hPa in 24 h. This is a slightly more modest deepening rate than the $24\sin\phi/\sin60°$ hPa in 24 h defined as an atmospheric bomb by Sanders and Gyakum (1980). It is chosen to permit the inclusion of the Great Storm of October 1987 (the storm only deepened a maximum 20.2 hPa in 24 h in the ERA-I simulation) within the class of explosively deepening cyclones. Of the 5447 cyclones, 22% develop explosively and 32% have a sting-jet precursor. This percentage of cyclones with a sting-jet precursor is very consistent with the 23–32 (dependent on the required size of the precursor region, between 8 and 5 grid points) of 100 cyclones found by Martínez-Alvarado et al. (2012) to have a sting-jet precursor using very similar methodology. Whereas 29% of the nonexplosively developing cyclones have a sting-jet precursor, 42% of those developing explosively have a precursor. Hence, cyclones are more likely to be explosively developing if they have a sting-jet precursor and vice versa.

Cyclones with and without sting-jet precursors have different frequency distributions in some parameters. Figures 3a and 3b show that distributions of MSLP deepening rate for cyclones with and without sting-jet precursors are similar, although there is a distinct tendency for explosively deepening cyclones to be more likely than nonexplosively deepening cyclones to have a sting-jet precursor, as shown quantitatively in Table 1.

If we consider only explosively deepening cyclones, the distribution of cyclone deepening rates is very similar whether or not the cyclone has a sting-jet precursor (Fig. 3b). By contrast, Figs. 3c and 3d show significantly different (above 99% level using a two-sample Kolmogorov–Smirnov test) distributions of maximum 850-hPa resolved wind speed and relative vorticity for cyclones with and without precursors. Hence, cyclones with a sting-jet precursor are more likely to have strong low-level resolved winds even in reanalysis data that are derived from a model that has too coarse resolution to be able to resolve mesoscale sting jets. Conversely, the majority of storms with extreme 850-hPa resolved winds (say $>55\,\mathrm{m\,s^{-1}}$) have a sting-jet precursor that would be expected to result in even more extreme gusts.

b. *Comparison of the spatial and seasonal cycle characteristics of cyclones with and without sting-jet precursors*

Track density is calculated at each grid point as the number of cyclones per month passing through a grid box per unit area equivalent to a 5° spherical cap ($\sim 10^6\,\mathrm{km^2}$) with each track being counted only once per spherical cap (after Hodges et al. 2011; Zappa et al. 2013). Figure 4a shows the storm-track density of all storms in this study. This is the characteristic North

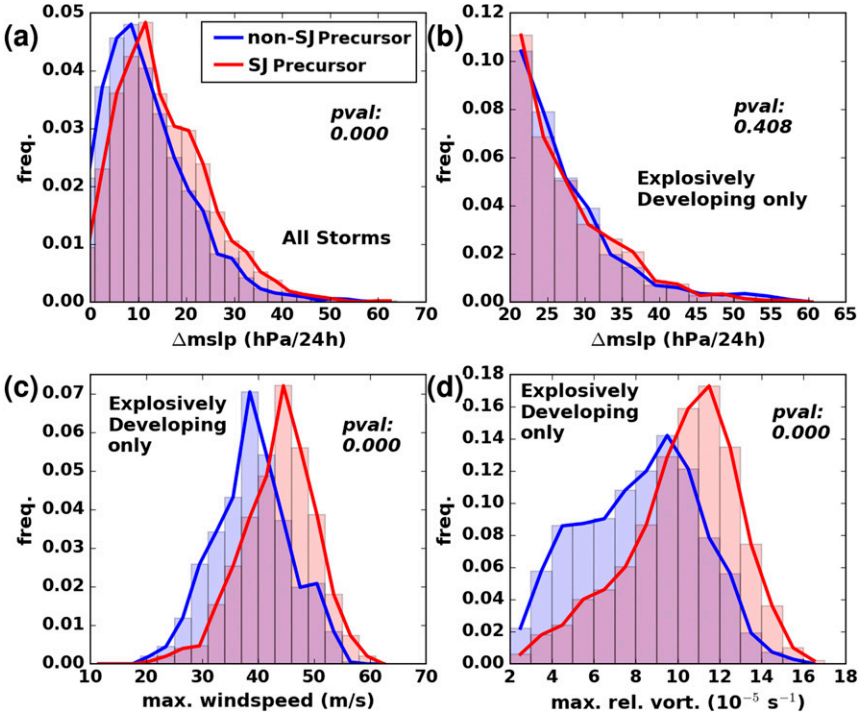

FIG. 3. Normalized frequency distributions of cyclone intensity metrics for North Atlantic cyclones with (red) and without (blue) the sting-jet precursor. (a) Distribution of the magnitude of the maximum drop in $MSLP_{min}$ for all North Atlantic cyclones. (b) As in (a), but for explosively developing ($\Delta MSLP_{min} < -20$ hPa over 24 h) cyclones only. The distribution of (c) the maximum 850-hPa resolved wind speed within 1000 km of the cyclone center and (d) the maximum 850 hPa relative vorticity. Distributions in (c) and (d) are for explosively developing cyclones only. Area under the normalized distributions integrates to 1. The p value from a Kolmogorov–Smirnov test indicating distinctness of the two distributions is shown to the third decimal on each panel.

Atlantic storm track [e.g., compare with Fig. 6b in Hoskins and Hodges (2002) and Fig. 2a in Dacre and Gray (2009)]. The most direct published comparison to Fig. 4 is Fig. 1a of Zappa et al. (2013) and Fig. 1a in Hodges et al. (2011), which shows December–February track density from the same reanalysis, ERA-I (1980–2009). Our values for track density are slightly lower than those shown by Zappa et al. (2013) because of our criterion that cyclones must reach their maximum intensity within a limited North Atlantic domain. The spatial distributions are shown for explosively developing cyclones only in Figs. 4b,c, subdivided into those cyclones with and without a sting-jet precursor; tracks of selected cyclones within these categories that have been described in published case studies are overlain on these panels. Up to 0.9 and more than 1.1 explosively developing cyclones per 5° hemispheric cap per month occur with and without sting-jet precursors, respectively. The storm track is more southerly and zonal for those cyclones with the precursors suggesting that environmental conditions, such as the greater moisture and warmth in the more southerly latitudes, affect the presence of DSCAPE in the cloud head of cyclones (as assessed by the precursor diagnostic).

For the named storms in Fig. 4, Table 2 gives references for published case studies and the maximum number of DSCAPE points diagnosed at any time during the evolution of the storm. Of the storms with a sting-jet precursor, the Great Storm of October 1987, and windstorms Gudrun, Friedhelm, and Robert have all been diagnosed as having a sting jet during their development. The storm from IOP4 of the ERICA field campaign has structural similarity to sting-jet windstorms suggesting that it may have had a sting jet. Martínez-Alvarado et al. (2014) discuss the observationally derived structural consistency between the ERICA storm and windstorm Friedhelm by reference to the ERICA storm case studies presented by Neiman and Shapiro (1993) and Neiman et al. (1993).

Of the storms without a sting-jet precursor, windstorm Tilo has been diagnosed as not having a sting jet, but

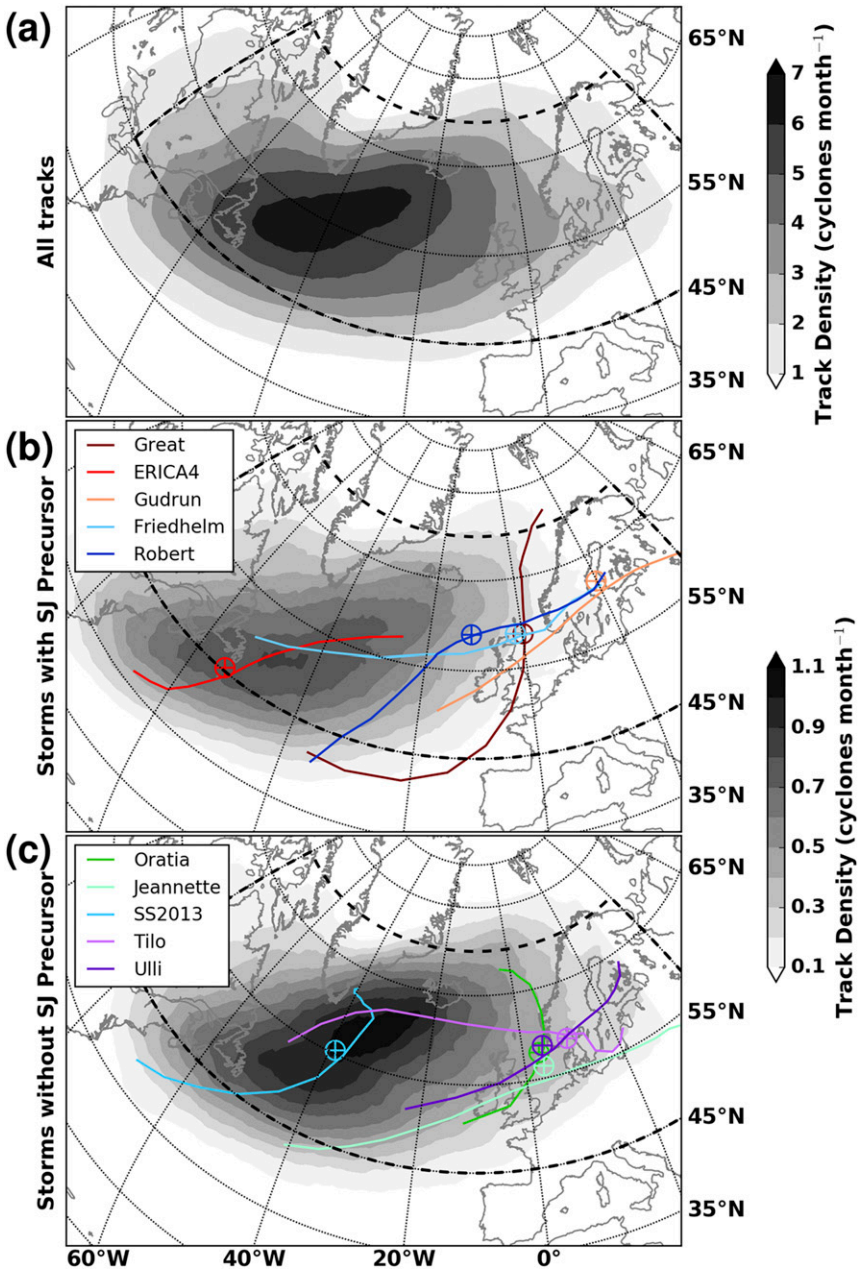

FIG. 4. Extratropical cyclone track density, defined as number density per month in a unit area equivalent to a 5° spherical cap (approximately 10^6 km^2) with cyclones counted only once per spherical cap, for cyclones occurring during September–May seasons through 1979–2012 with vorticity maxima within the dashed black curve. (a) Track density for all cyclones. Track density for explosively developing ($\Delta MSLP_{min} < -20$ hPa over 24 h) cyclones (b) without and (c) with sting-jet precursors; selected tracks (based on ζ_{850} with locations of lowest MSLP marked by circles with plus sign) from cyclones with published case studies are shown by colored lines with legend.

windstorms Ulli, Jeanette, and the 2005 storm labeled SS2013 have all been diagnosed as having sting jets. While these storms did not pass the DSCAPE threshold set in section 2 and displayed in Fig. 5, DSCAPE was nevertheless present (Table 2). It is clear from Fig. 5 that storms with few valid DSCAPE grid volumes are much more common than storms such as the ERICA IOP4 storm or the Great Storm of October 1987. As noted in the methodology section, the threshold of five DSCAPE points provided a high identification rate of

TABLE 2. Number of model grid points with DSCAPE diagnosed in each historical storm plotted in Fig. 4.

	No. of DSCAPE points	Date	References
Great Storm	37	15 Oct 1987	Browning (2005) and Clark et al. (2005)
ERICA IOP4	13	4 Jan 1989	Neiman et al. (1993) and Neiman and Shapiro (1993)
Oratia	0	30 Oct 2000	Browning (2005) and Hewson and Neu (2015)
Jeannette	4	17 Oct 2002	Parton et al. (2009)
Gudrun	16	7 Jan 2005	Baker (2009) and Gray et al. (2011)
SS2013	6	8 Dec 2005	Schultz and Sienkiewicz (2013)
Tilo	2	07 Nov 2007	Gray et al. (2011)
Friedhelm	23	8 Dec 2011	Martínez-Alvarado et al. (2014)
Robert	10	16 Dec 2011	—
Ulli	2	2 Jan 2012	Smart and Browning (2014)

sting-jet-producing storms as demonstrated in Martínez-Alvarado et al. (2013). Thus, the choice of eight points in this study is more conservative and likely to miss more marginal cases. The lack of CSI for windstorm Ulli is consistent with the conclusion of Smart and Browning (2014) that "CSI did not play a major role" in the descending sting jet. The conclusion of the study of SS2013 in Schultz and Sienkiewicz (2013) was that forcing associated with frontolysis drives the descent of air in this storm. Results here show that CSI was however present in the reanalysis with six DSCAPE grid volumes identified (Table 2).

The sting-jet precursor diagnostic failed to flag windstorm Jeanette (four DSCAPE points) as a possible sting-jet storm. It is worth noting though that while Parton et al. (2009) showed clear evidence of a sting jet in windstorm Jeanette (from observations and trajectory analysis using model data), Hewson and Neu (2015) assert that the cold conveyor belt was the cause of the strongest gusts over land in this storm (from observations and synoptic chart analysis). We also note that while Hewson and Neu (2015) assert that the sting jet was one of the causes of the strongest gusts over land in windstorm Oratia, there is no published study on this storm, to our knowledge, in which the presence of a sting jet is diagnosed from trajectory analysis (arguably the only way to rigorously diagnose a descending jet).

Figure 6 shows that explosive cyclones with sting-jet precursors have a more marked seasonal cycle than those without precursors. The numbers of North Atlantic cyclones with precursors are markedly greater in December, January, and February compared to the other months, increasing to a mean of about 3 cyclones month^{-1} compared to less than 2 cyclones month^{-1} for the other months. In contrast, the numbers of cyclones without a precursor peak slightly earlier in the winter season and have a much flatter seasonal cycle with the maximum of the monthly means reaching a slightly lower number than that for the cyclones with precursors. Although these results suggest that December–February is the most dangerous time for strong resolved winds associated with sting-jet cyclones, several notable sting-jet cyclones have occurred that impacted the British Isles outside these months including the Great Storm of October 1987 (e.g., Browning 2005) and windstorm Christian (also known as the St Jude's day storm, October 2013; Browning et al. 2015).

The most significant difference is the absence of cyclones with sting-jet precursors in March–May. Further research is needed to determine the cause and significance of this difference in seasonal cycles for cyclones with and without precursors.

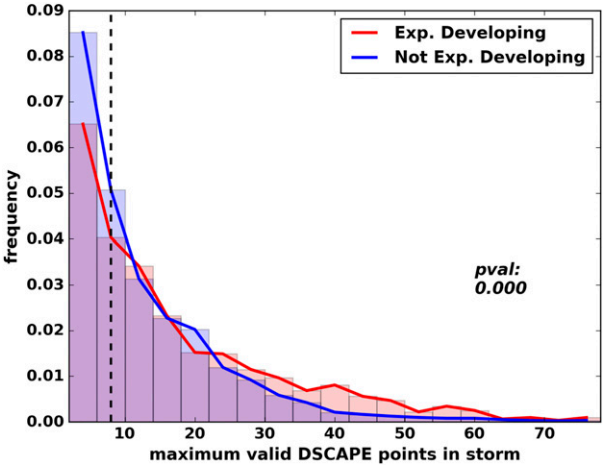

FIG. 5. Normalized frequency distribution showing the maximum number of valid cloud head DSCAPE grid volumes produced during North Atlantic extratropical cyclone life cycles in ERA-I. Only storms that produced at least two DSCAPE points are included. Distributions of DSCAPE points produced in explosively (red) and nonexplosively (blue) developing cyclones are shown separately. The black dashed line shows the threshold of eight DSCAPE points used in this study to flag storms with potential to produce sting jets. The p value from a Kolmogorov–Smirnov test is zero when rounded to third decimal, indicating the distributions are statistically distinct.

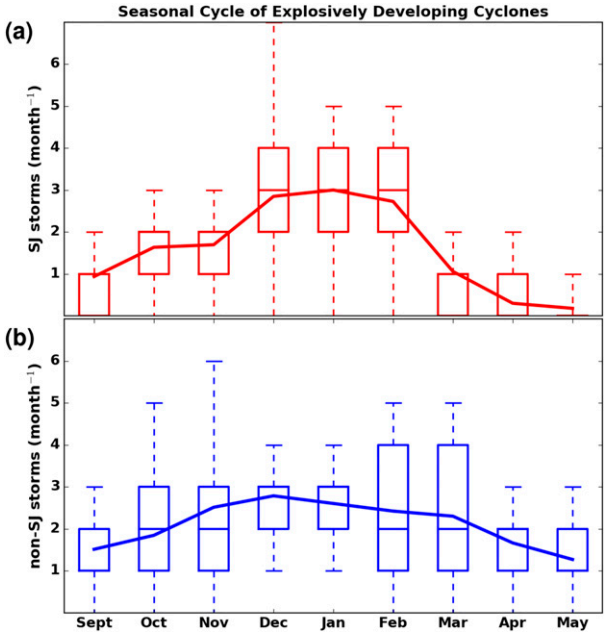

FIG. 6. The seasonal cycle (September–May) in number of explosively developing cyclone in the domain defined in Fig. 4 for cyclones (a) with and (b) without sting-jet precursors. Lines join the monthly mean values; the top and bottom of the boxes denote first and third quartile of cyclone numbers, while whiskers show full range of cyclone numbers for each month.

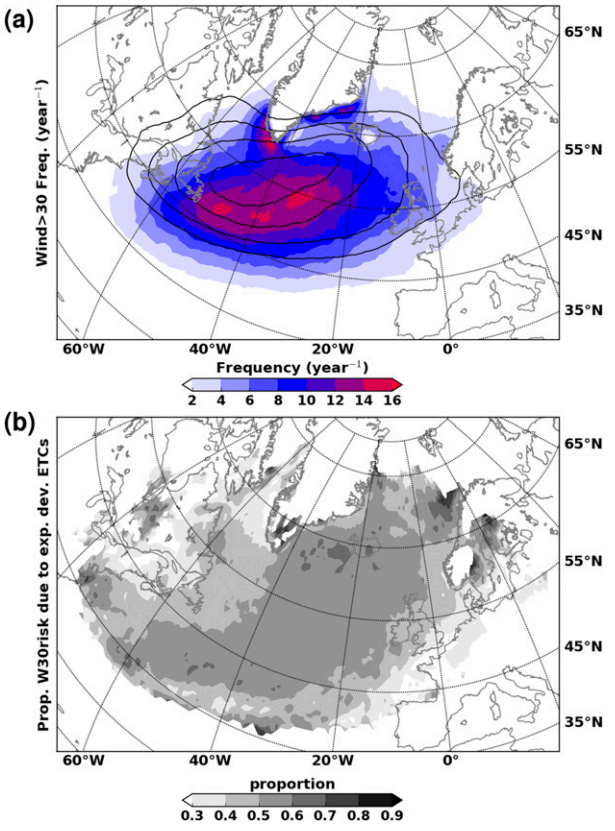

FIG. 7. (a) The annual frequency of 850-hPa resolved wind speeds $>30\,m\,s^{-1}$ within 1000 km of tracked cyclone centers computed from all storms (shaded); contours mark the 2–6 (increment 1) cyclones month^{-1} track density, taken from Fig. 4a. (b) The proportion of the frequency in (a) due to the wind swaths of explosively developing cyclones; data at points where the total number of tracked cyclones is fewer than 10 are masked out.

c. *Comparison of the resolved wind distribution characteristics of cyclones with and without sting-jet precursors*

The frequency distributions for the maximum 850-hPa resolved wind speed and relative vorticity (Fig. 3) show that cyclones with sting-jet precursors are more likely to have strong resolved winds (and the related relative vorticity) than those without. The spatial distributions of these resolved winds are now analyzed. A map of the annual frequency of 850-hPa resolved wind speeds exceeding $30\,m\,s^{-1}$ for all cyclones is shown in Fig. 7a. This is calculated using the wind footprints of the cyclones (within 1000 km of the cyclones' MSLP-derived centers). The band of high resolved wind speed frequency lies to the south of the band of strong track density (shown by the contours in Fig. 7a). This is consistent with the strongest resolved wind speeds in cyclones typically being found to the south of the cyclone center due to the greater similarity between environmental and cyclone wind directions here. High frequencies of strong resolved winds associated with the tracked cyclones are also found along the Greenland coastline, particularly toward the southern tip of the west coast. The interaction of synoptic-scale cyclones with the high topography of Greenland can lead to mesoscale cyclogenesis or bands of strong resolved winds. However, the observation-based climatology of Moore and Renfrew (2005) shows that tip jets, reverse tip jets, and barrier winds are associated with strong winds along the east coast and at, and to the south of, the tip of Greenland; the paper shows there is no observed climatological (averaged over 5 yr) maxima in mean 10-m wind speed along the west coast. Hence, it is possible that the high frequency of strong resolved winds diagnosed along the west coast here is an artifact of the data due to the presence of orography (or due to considering 850-hPa rather than 10-m resolved wind speeds) rather than a real signal. The proportion of the strong resolved wind frequency (exceeding $30\,m\,s^{-1}$) associated with explosively developing cyclones is shown in Fig. 7b. This proportion is remarkably consistent across the domain, ranging from 40% to 60%. Very high proportions at the edges are an effect resulting from small sample sizes. There is also a large area where 50%–60% of the events are associated with explosively developing cyclones

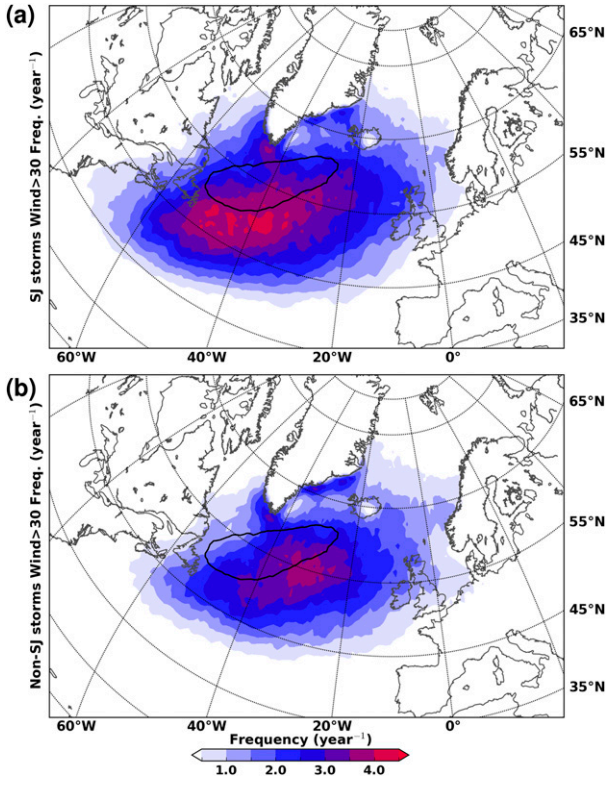

FIG. 8. The annual frequency of 850-hPa resolved wind speeds $>30\,\mathrm{m\,s^{-1}}$ within 1000 km of tracked cyclone centers (shaded) computed from the 850-hPa resolved wind swaths of explosively deepening cyclones only and separated into cyclones (a) with and (b) without sting-jet precursors. Track density contour of 6 cyclones $\mathrm{month^{-1}}$ (from Fig. 4a) shown for reference.

across a broad latitude band (about 40°–65°N) east of 40°W.

The resolved wind frequency distributions differ for the explosively developing cyclones with and without sting-jet precursors (Fig. 8). The band of high frequencies is much larger for the cyclones with sting-jet precursors (e.g., compare the regions where the frequencies exceed 3 events per year in Figs. 8a,b). The greater contribution of cyclones with sting-jet precursors to strong resolved wind events is striking given that these cyclones account for less than half (42%) of the explosively developing cyclones. The additional region of high resolved wind frequencies for the cyclones with sting-jet precursors is found as an extension to the southwest of the high resolved wind frequency region for the cyclones without sting-jet precursors. The importance of cyclones with sting-jet precursors for strong resolved winds in the southwestern North Atlantic is consistent with the more southerly storm track of explosively developing cyclones with sting-jet precursors compared to those without precursors (Fig. 4).

Figure 9 shows the contribution of explosively developing cyclones with and without sting-jet precursors to the frequency of strong resolved wind events partitioned further, into the proportional contributions of resolved winds found in the cool and warm sectors of both types of cyclones to the total frequency of strong resolved wind events associated with explosively developing cyclones. Strong resolved winds, as defined here, occur almost entirely in the cool sector of cyclones and are hence associated with the cold conveyor belt jet: less than 30% of the events occur in the warm sectors except for off the eastern Canadian coast for cyclones with sting-jet precursors (although the identification of the fronts, and hence cool warm and sectors, may be less reliable here as a result of the orography). Consistent with Fig. 8, there is a large difference between the cyclones with and without sting-jet precursors. Cyclones with precursors contribute nearly 100% of the strong resolved wind events in the southwestern North Atlantic (Fig. 9). The contributions from both types of cyclones are about equal in the mid-Atlantic (within about 55°–65°N, 40°W–0°). Cyclones without precursors dominate in the northeast of the data region and over northwestern continental Europe. However, the relative contributions of the cool sectors of explosively developing cyclones with and without sting-jet precursors to the frequencies of strong resolved wind events is highly dependent on the threshold used to define "strong." Figure 10 shows the equivalent of Figs. 9a,c (i.e., cool-sector resolved winds), but for 850-hPa resolved wind speed thresholds of 25 and $35\,\mathrm{m\,s^{-1}}$ instead of $30\,\mathrm{m\,s^{-1}}$.

The overall pattern of proportional contributions holds for all three resolved wind speed thresholds: precursors make a greater contribution in the southwestern North Atlantic than in the northeastern North Atlantic and northeastern continental Europe and vice versa for the cyclones without precursors. However, the contribution of cyclones with precursors to the frequency of strong resolved wind events increases throughout the North Atlantic with increasing resolved wind speed threshold. For the resolved wind speed threshold of $35\,\mathrm{m\,s^{-1}}$, the cool sectors of cyclones with sting-jet precursors account for more than 70% of strong resolved wind events over some parts of the British Isles (these high percentages may extend over southern England but could not be calculated here because of a paucity of such events in the dataset). These high percentages imply that the strongest resolved wind events occurring over the British Isles are highly likely to be due to cyclones that have sting-jet precursors. Conversely, over northwestern continental Europe strong resolved wind speed events are most likely to be due to cyclones that do not have sting-jet precursors although events with 850-hPa resolved wind speeds exceeding $35\,\mathrm{m\,s^{-1}}$ are rare.

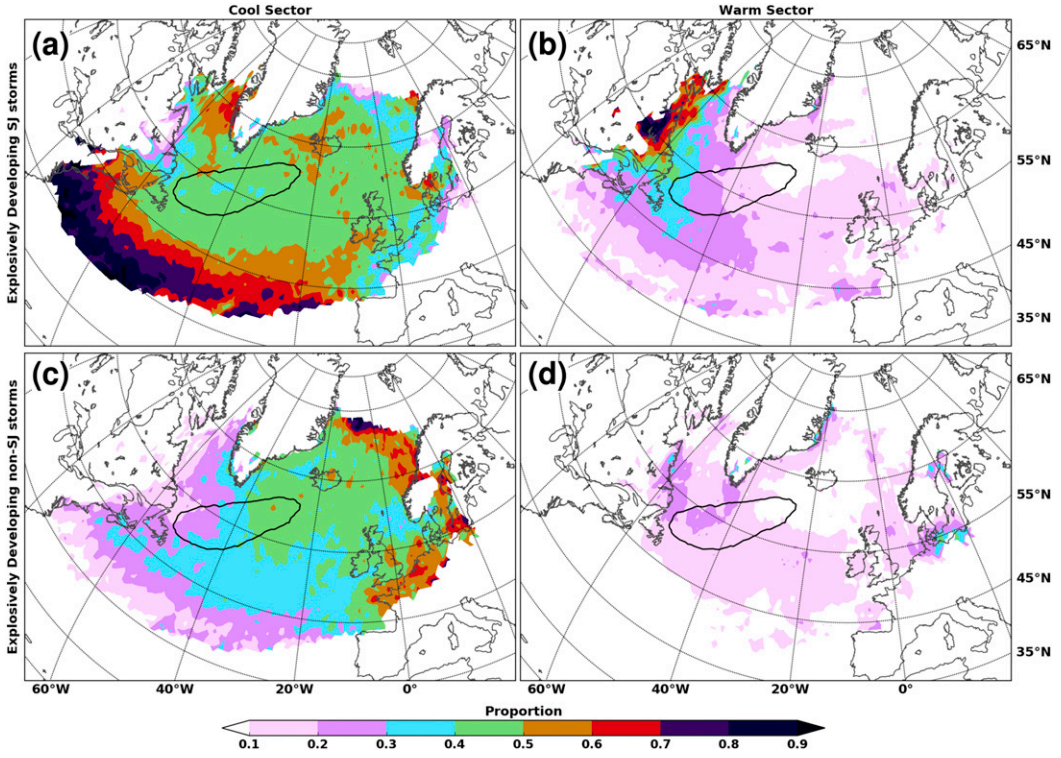

FIG. 9. The proportion of the annual frequency of 850-hPa resolved wind speeds $>30\,\mathrm{m\,s^{-1}}$ within 1000 km of tracked cyclone centers computed from explosively deepening cyclones only (i.e., sum of frequencies shown in Figs. 8a,b) due to cyclones (a),(b) with and (c),(d) without sting-jet precursor and found within the (a),(c) cool and (b),(d) warm sectors of the cyclones. Track density contour of 6 cyclones $\mathrm{month^{-1}}$ (from Fig. 4a) shown for reference.

Figure 11 shows this difference in relative importance of storms with sting-jet precursors for strong resolved winds over the British Isles and northwestern continental Europe for a wider range of resolved wind speed thresholds in terms of spatially averaged frequencies. The frequency of strong resolved wind events of course decreases with resolved wind speed threshold for all types of cyclones and in both regions (Figs. 11a,c), but the proportion of resolved wind risk from each type of cyclone is highly wind speed threshold dependent. For a wind speed threshold of $\geq 30\,\mathrm{m\,s^{-1}}$ over the British Isles, strong resolved wind events are increasingly likely to be caused by explosively developing storms with a sting-jet precursor. This type of storm is associated with more than 60% of all events for the strongest resolved wind speed threshold considered ($45\,\mathrm{m\,s^{-1}}$); including also the nonexplosively developing storms with a precursor increases this proportion to more than 80%. Explosively developing precursor storms are also the most prevalent for the northwestern continental Europe region for the strongest wind speed threshold (Fig. 11d). However, there are far fewer strong resolved wind events for the northwestern continental Europe region than for the British Isles (cf. Figs. 11a and 11c), so these results may be affected by sampling error. For the midrange resolved wind speed threshold ($35\,\mathrm{m\,s^{-1}}$), strong resolved wind events over the northwestern continental Europe region are most likely to not develop explosively and not have a sting-jet precursor and least likely to be explosively developing storms with a sting-jet precursor.

4. Discussion and conclusions

The aim of this study is to produce a climatology of sting-jet cyclones and assess their contribution to strong near-surface winds. The long period of data required to produce a climatology naturally leads to the use of reanalysis data. However, the resolution of models used to produce reanalyses is too coarse to resolve these transient mesoscale jets. Hence, instead of diagnosing the presence of sting jets directly, precursors of sting jets have been diagnosed. A sting-jet precursor is identified if there is sufficient atmospheric instability (using the metric DSCAPE) in the hooked tip of the cloud head of a cyclone.

The sting-jet precursor diagnostic has been applied to all tracked North Atlantic cyclones in the ERA-I dataset

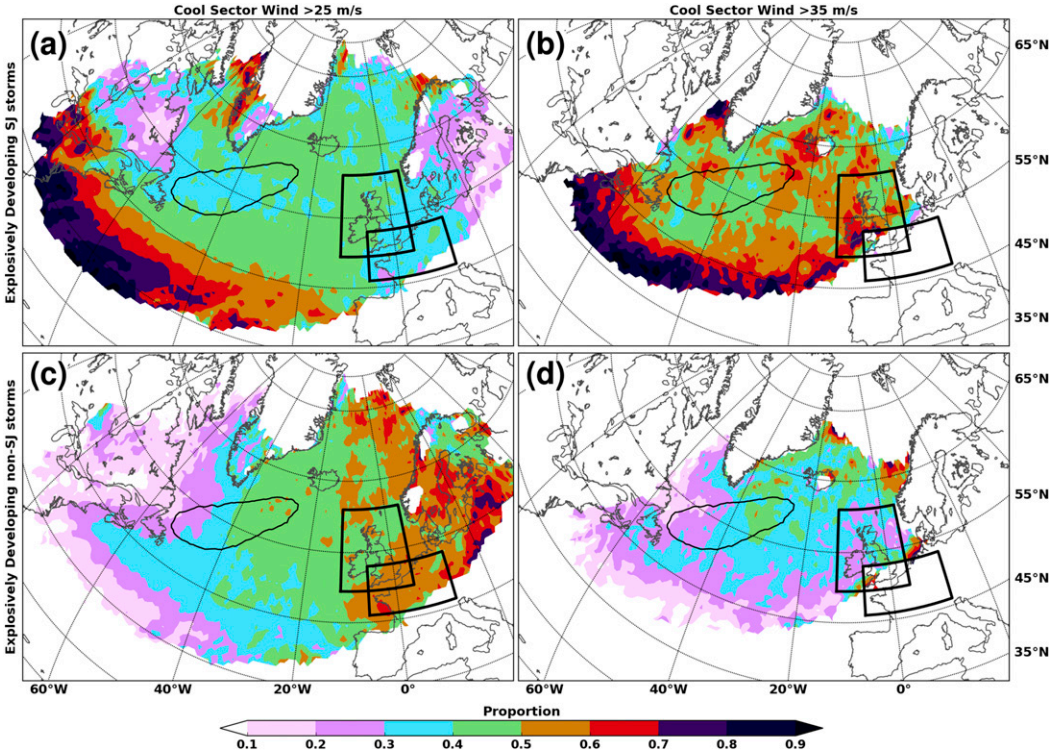

FIG. 10. As in Fig. 9, but showing only cool-sector resolved winds proportions for cyclones (a),(b) with and (c),(d) without sting-jet precursors calculated from the frequencies of 850-hPa resolved wind speeds exceeding (a),(c) 25 and (b),(d) 35 m s^{-1}. Boxes marked on the panels show the U.K. and continental western Europe domains used in Fig. 11.

from 1979 to 2012. A previous study (Martínez-Alvarado et al. 2012) demonstrated that (i) this diagnostic has skill in the identification of extratropical cyclones that produce sting jets in weather forecast simulations with sufficient resolution to resolve sting jets and (ii) up to about a third of extratropical cyclones (based on a sample of 100 cyclones from the ERA-I dataset) exhibit the sting-jet precursor and so are inferred to have had sting jets. Here we extend this previous study to consider all cyclones from 32 extended winter seasons of ERA-I data and consider the resolved wind risk associated with sting-jet cyclones.

Of the 5447 extratropical cyclones tracked, 32% had a sting-jet precursor; this increased to 42% in the 22% of cyclones that developed explosively (defined here as deepening by 20 hPa in 24 h). The consistency between the percentage of all cyclones found to have had a sting-jet precursor in this study and in the study of Martínez-Alvarado et al. (2012) is reassuring given the almost identical methodology. A greater percentage of explosively developing than nonexplosively developing cyclones have sting-jet precursors (42% compared to 29%), and the wind damage potential of explosively developing storms motivated the focus of the remainder of the paper on these storms. It is in the cyclone intensity metric of maximum 850-hPa resolved wind speed (and associated maximum 850-hPa relative vorticity), rather than MSLP fall, that the most notable difference between the distributions for cyclones with and without sting-jet precursors is seen: the resolved wind speed distribution is displaced to significantly higher values for the cyclones with precursors.

The spatial distribution of explosively developing cyclones with and without sting-jet precursors are different, with cyclones with precursors having more southerly and zonal storm tracks (revealed by track density maps). This is consistent with the requirement of warm moist air to generate CSI and a substantial cloud head and with the finding of Martínez-Alvarado et al. (2012) that the start locations of tracks were farther south for cyclones with precursors compared to those without. Explosively developing cyclones with precursors also have a stronger seasonal cycle that peaks in December, January, and February at about 3 cyclones $month^{-1}$ on average; the reason for this requires further investigation.

The risk of wind-induced damage resulting from sting-jet cyclones is the primary motivator for studying them.

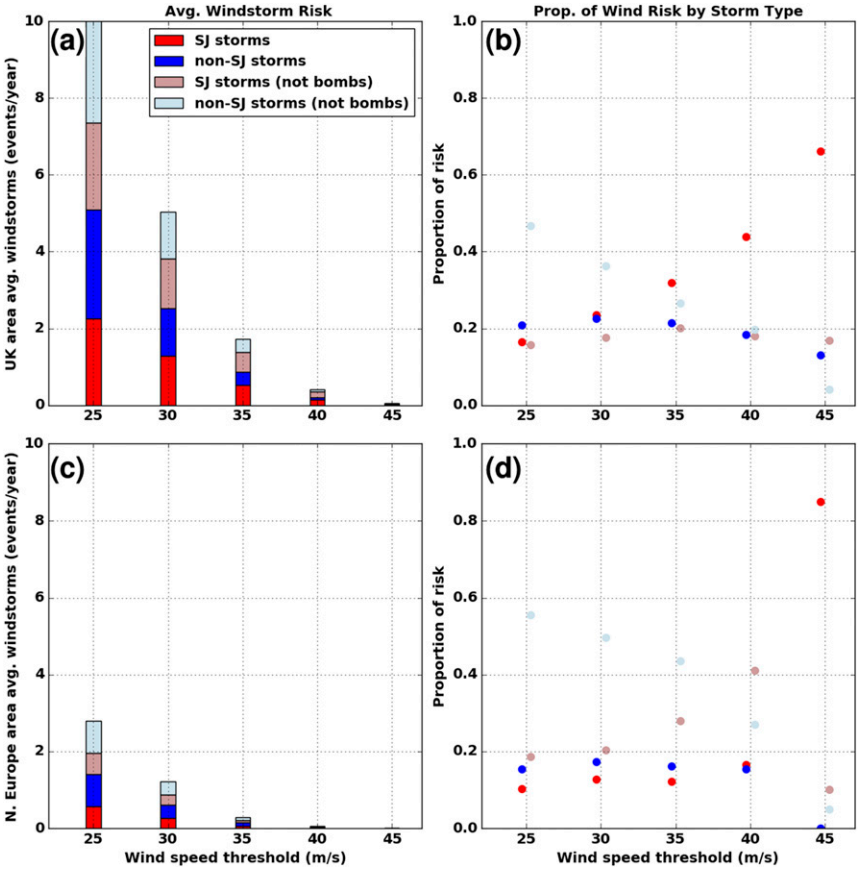

FIG. 11. (a) Frequency (events yr^{-1}) of strong resolved wind events in storms with (red shading) and without (blue shading) sting-jet precursors averaged over the U.K. domain (marked in Fig. 10) for resolved wind speed thresholds from 25 to 45 m s^{-1} (increment 5 m s^{-1}). Distinction is made between storms that did (dark shading) and did not (light shading) develop explosively. (b) As in (a), but data plotted as a proportion of total frequencies for each resolved wind speed threshold. (c),(d) As in (a),(b), but for the continental western European domain (marked in Fig. 10). Some of the points in (b) and (d) are displaced slightly from the resolved wind speed threshold lines for clarity.

We have justified the use the resolved wind speed at 850 hPa as a simple and easily obtainable, but realistic, estimate of the most damaging wind gusts at the surface. The resolved wind frequency maps presented here show that more than 12 cyclone-related strong resolved wind events per year (defined as 850-hPa resolved wind speed exceeding 30 m s^{-1}) occur in a broad band in the western North Atlantic; over the British Isles between 2 and 8 such events occur per year with the number increasing from south to north. Explosively developing cyclones account for about half of these events across most of the North Atlantic and extending over the British Isles. There is a stark difference between the resolved wind speed frequency maps for the explosively developing cyclones with and without sting-jet precursors. While the maps are similar over the British Isles and mid–North Atlantic, cyclones with precursors dominate the events in the southwestern North Atlantic (where the explosively developing cyclone track density is dominated by cyclones with precursors). It has further been shown that the vast majority of strong resolved wind events associated with explosively developing cyclones are occurring in the cool sectors of cyclones. Furthermore, storms generating strong resolved winds over the British Isles are most likely to be explosively developing and have sting-jet precursors (for 850-hPa resolved wind speeds $\geq$35 m s^{-1}).

The stronger resolved wind speeds found for cyclones with sting-jet precursors seem to present a paradox. The model used to generate the ERA-I dataset has too coarse resolution to resolve sting jets and yet cyclones with a sting-jet precursor have stronger low-level resolved winds. The resolution of this paradox comes from the interpretation that the strong resolved winds

occurring in the cool sectors of cyclones are due to cold conveyor belt jets rather than sting jets. There are four reasons why the presence of a sting-jet precursor may be associated with a stronger cold conveyor belt jet:

1) Cyclones with the precursor have atmospheric instability in their cloud heads that is likely to be released by the model dynamics if it reaches a sufficient level of instability, although this release may not be physically realistic (e.g., the CSI could eventually be converted to CI and released through the convection scheme; Gray et al. 2011).
2) Cyclones with the DSCAPE precursor (and so CSI) are probably more likely to have substantial cloud heads (Shutts 1990), an indicator of rapidly developing cyclones (e.g., Bader et al. 1995), which are generally associated with strong cold conveyor belt jets.
3) The more southerly storm tracks of cyclones with the precursor will likely enhance the heating occurring in the warm conveyor belt and Schemm and Wernli (2014) demonstrated that this heating increases the potential vorticity in the cold conveyor belt, indirectly driving the associated jet.
4) The precursor identifies frontal zones where the saturated equivalent potential temperature and absolute momentum surfaces are close to parallel, an indicator of strong baroclinicity and so strong frontal gradients along the bent-back fronts and hence strong cold conveyor belt jets.

In summary, the sting-jet precursor diagnostic thus identifies cyclones that are likely to have a more southerly and zonal storm track and are the main cause of strong resolved wind events in the southwestern North Atlantic. Even over the British Isles these cyclones account for about half of all strong 850-hPa resolved wind events exceeding $30\,m\,s^{-1}$; this value increases to more than 80% when the resolved wind speed threshold is increased to $45\,m\,s^{-1}$ and when cyclones developing both explosively and nonexplosively are considered. In contrast, cyclones without precursors are the most likely cause of cyclone-related strong resolved wind events over northwestern continental Europe (more than 50% of events are found in the cool sectors of these cyclones for resolved wind speed thresholds of 25 and $35\,m\,s^{-1}$; resolved wind speed events exceeding $35\,m\,s^{-1}$ are rare). In reality, cyclones with sting-jet precursors are likely to have had a sting jet that is not represented in the reanalysis data analyzed here. The presence of the sting jet is likely to further enhance the resolved winds in the cool sector of the cyclone either directly, if the sting jet descends ahead of the cold conveyor belt jet, or indirectly, if the sting jet descends above the cold conveyor belt jet and enhances it through momentum transfer into the boundary layer; this momentum transfer was found to happen through convective circulations by Browning et al. (2015) for the St Jude's day storm (October 2013) and the boundary layer is typically unstable in the region of the cold conveyor belt as a result of the comparatively warm winter ocean (Sinclair et al. 2010; Hewson and Neu 2015). In conclusion, the sting-jet precursor diagnostic is a powerful tool to identify cyclones likely to be associated with damaging resolved winds and indicate possible underprediction of surface wind speed and gusts as a result of insufficient model resolution.

Acknowledgments. We are grateful to ECMWF for the provision of the ERA-Interim dataset and to Kevin Hodges (University of Reading) for provision of the cyclone tracks. Oscar Martínez-Alvarado is thanked for his support in the calculation of the sting-jet precursor diagnostic, including provision of some code. Three anonymous reviewers are thanked for their comments. This work was supported by the AXA-Research Fund under the Project "Sting Jet Windstorms in Current and Future Climates." Neil C. G. Hart has ORCID iD orcid.org/0000-0002-6902-8699, Suzanne L. Gray has ORCID iD orcid.org/0000-0001-8658-362X, and Peter A. Clark has ORCID iD orcid.org/0000-0003-1001-9226.

REFERENCES

Bader, M. J., G. S. Forbes, J. R. Grant, R. B. E. Lilley, and A. J. Waters, Eds., 1995: *Images in Weather Forecasting: A Practical Guide for Interpreting Satellite and Radar Imagery*. Cambridge University Press, 523 pp.

Baker, L. H., 2009: Sting jets in severe northern European wind storms. *Weather*, **64**, 143–148, doi:10.1002/wea.397.

Browning, K. A., 2004: The sting at the end of the tail: Damaging winds associated with extratropical cyclones. *Quart. J. Roy. Meteor. Soc.*, **130**, 375–399, doi:10.1256/qj.02.143.

——, 2005: Observational synthesis of mesoscale structures within an explosively developing cyclone. *Quart. J. Roy. Meteor. Soc.*, **131**, 603–623, doi:10.1256/qj.03.201.

——, D. J. Smart, M. R. Clark, and A. J. Illingworth, 2015: The role of evaporating showers in the transfer of sting-jet momentum to the surface. *Quart. J. Roy. Meteor. Soc.*, **141**, 2956–2971, doi:10.1002/qj.2581.

Burt, S. D., and D. A. Mansfield, 1988: The Great Storm of 15–16 October 1987. *Weather*, **43**, 90–110, doi:10.1002/j.1477-8696.1988.tb03885.x.

Catto, J. L., L. C. Shaffrey, and K. I. Hodges, 2010: Can climate models capture the structure of extratropical cyclones? *J. Climate*, **23**, 1621–1635, doi:10.1175/2009JCLI3318.1.

Clark, P. A., K. A. Browning, and C. Wang, 2005: The sting at the end of the tail: Model diagnostics of the fine-scale three-dimensional structure of the cloud band. *Quart. J. Roy. Meteor. Soc.*, **131**, 2263–2292, doi:10.1256/qj.04.36.

Dacre, H. F., and S. L. Gray, 2009: The spatial distribution and evolution characteristics of North Atlantic cyclones. *Mon. Wea. Rev.*, **137**, 99–115, doi:10.1175/2008MWR2491.1.

Dee, D. P., and Coauthors, 2011: The ERA-Interim reanalysis: Configuration and performance of the data assimilation system. *Quart. J. Roy. Meteor. Soc.*, **137**, 553–597, doi:10.1002/qj.828.

Emanuel, K. A., 1994: *Atmospheric Convection*. Oxford University Press, 580 pp.

Fink, A. H., T. Brücher, V. Ermert, A. Krüger, and J. G. Pinto, 2009: The European storm Kyrill in January 2007: Synoptic evolution, meteorological impacts and some considerations with respect to climate change. *Nat. Hazards*, **9**, 405–423, doi:10.5194/nhess-9-405-2009.

Gray, S. L., O. Martínez-Alvarado, L. H. Baker, and P. A. Clark, 2011: Conditional symmetric instability in sting jet storms. *Quart. J. Roy. Meteor. Soc.*, **137**, 1482–1500, doi:10.1002/qj.859.

Grønås, S., 1995: The seclusion intensification of the New Year's Day storm 1992. *Tellus*, **47A**, 733–746, doi:10.3402/tellusa.v47i5.11571.

Hewson, T., and U. Neu, 2015: Cyclones, windstorms and the IMILAST project. *Tellus*, **67A**, 27128, doi:10.3402/tellusa.v67.27128.

Hodges, K. I., 1994: A general method for tracking analysis and its application to meteorological data. *Mon. Wea. Rev.*, **122**, 2573–2586, doi:10.1175/1520-0493(1994)122<2573:AGMFTA>2.0.CO;2.

——, 1995: Feature tracking on the unit sphere. *Mon. Wea. Rev.*, **123**, 3458–3465, doi:10.1175/1520-0493(1995)123<3458:FTOTUS>2.0.CO;2.

——, R. W. Lee, and L. Bengtsson, 2011: A comparison of extratropical cyclones in recent reanalyses ERA-Interim, NASA MERRA, NCEP CFSR, AND JRA-25. *J. Climate*, **24**, 4888–4906, doi:10.1175/2011JCLI4097.1.

Hoskins, B. J., and K. I. Hodges, 2002: New perspectives on the Northern Hemisphere winter storm tracks. *J. Atmos. Sci.*, **59**, 1041–1061, doi:10.1175/1520-0469(2002)059<1041:NPOTNH>2.0.CO;2.

Martínez-Alvarado, O., S. L. Gray, J. L. Catto, and P. A. Clark, 2012: Sting jets in intense North-Atlantic windstorms. *Environ. Res. Lett.*, **7**, 024014, doi:10.1088/1748-9326/7/2/024014; Corrigendum, **9**, 039501, doi:10.1088/1748-9326/9/3/039501.

——, ——, P. A. Clark, and L. H. Baker, 2013: Objective detection of sting jets in low-resolution datasets. *Meteor. Appl.*, **20**, 41–55, doi:10.1002/met.297.

——, L. H. Baker, S. L. Gray, J. Methven, and R. S. Plant, 2014: Distinguishing the cold conveyor belt and sting jet air streams in an intense extratropical cyclone. *Mon. Wea. Rev.*, **142**, 2571–2595, doi:10.1175/MWR-D-13-00348.1.

Moore, G. W. K., and I. A. Renfrew, 2005: Tip jets and barrier winds: A QuikSCAT climatology of high wind speed events around Greenland. *J. Climate*, **18**, 3713–3725, doi:10.1175/JCLI3455.1.

Murray, R. J., and I. Simmonds, 1991: A numerical scheme for tracking cyclone centres from digital data. Part 1: Development and operation of the scheme. *Aust. Meteor. Mag.*, **39**, 155–166.

Neiman, P. J., and M. Shapiro, 1993: The life cycle of an extratropical marine cyclone. Part I: Frontal-cyclone evolution and thermodynamic air–sea interaction. *Mon. Wea. Rev.*, **121**, 2153–2176, doi:10.1175/1520-0493(1993)121<2153:TLCOAE>2.0.CO;2.

——, ——, and L. Fedor, 1993: The life cycle of an extratropical marine cyclone. Part II: Mesoscale structure and diagnostics. *Mon. Wea. Rev.*, **121**, 2177–2199, doi:10.1175/1520-0493(1993)121<2177:TLCOAE>2.0.CO;2.

Panofsky, H. A., H. Tennekes, D. H. Lenschow, and J. C. Wyngaard, 1977: The characteristics of turbulent velocity components in the surface layer under convective conditions. *Bound.-Layer Meteor.*, **11**, 355–361, doi:10.1007/BF02186086.

Parton, G. A., G. Vaughan, E. G. Norton, K. A. Browning, and P. A. Clark, 2009: Wind profiler observations of a sting jet. *Quart. J. Roy. Meteor. Soc.*, **135**, 663–680, doi:10.1002/qj.398.

Pirret, J. S. R., P. Knippertz, and T. M. Trzeciak, 2017: Drivers for the deepening of severe European windstorms and their impacts on forecast quality. *Quart. J. Roy. Meteor. Soc.*, **143**, 309–320, doi:10.1002/qj.2923.

Roberts, J. F., and Coauthors, 2014: The XWS open access catalogue of extreme European windstorms from 1979 to 2012. *Nat. Hazards*, **14**, 2487–2501, doi:10.5194/nhess-14-2487-2014.

Sanders, F., and J. R. Gyakum, 1980: Synoptic-dynamic climatology of the "bomb." *Mon. Wea. Rev.*, **108**, 1589–1606, doi:10.1175/1520-0493(1980)108<1589:SDCOT>2.0.CO;2.

Schemm, S., and H. Wernli, 2014: The linkage between the warm and the cold conveyor belts in an idealized extratropical cyclone. *J. Atmos. Sci.*, **71**, 1443–1459, doi:10.1175/JAS-D-13-0177.1.

Schultz, D. M., 2001: Reexamining the cold conveyor belt. *Mon. Wea. Rev.*, **129**, 2205–2225, doi:10.1175/1520-0493(2001)129<2205:RTCCB>2.0.CO;2.

——, and J. M. Sienkiewicz, 2013: Using frontogenesis to identify sting jets in extratropical cyclones. *Wea. Forecasting*, **28**, 603–613, doi:10.1175/WAF-D-12-00126.1.

Shapiro, M. A., and D. A. Keyser, 1990: Fronts, jet streams, and the tropopause. *Extratropical Cyclones: The Erik Palmén Memorial Volume*, C. W. Newton and E. O. Holopainen, Eds., Amer. Meteor. Soc., 167–191.

Sheridan, P., 2011: Review of techniques and research for gust forecasting and parameterisation. Met Office Forecasting Research Tech. Rep. 570, 20 pp.

Shutts, G., 1990: Dynamical aspects of the October storm, 1987: A study of a successful fine-mesh simulation. *Quart. J. Roy. Meteor. Soc.*, **116**, 1315–1347, doi:10.1002/qj.49711649604.

Simmonds, I., and K. Keay, 2000: Mean Southern Hemisphere extratropical cyclone behavior in the 40-year NCEP–NCAR reanalysis. *J. Climate*, **13**, 873–885, doi:10.1175/1520-0442(2000)013<0873:MSHECB>2.0.CO;2.

Sinclair, V., S. Belcher, and S. Gray, 2010: Synoptic controls on boundary-layer characteristics. *Bound.-Layer Meteor.*, **134**, 387–409, doi:10.1007/s10546-009-9455-6.

Smart, D. J., and K. A. Browning, 2014: Attribution of strong winds to a cold conveyor belt and sting jet. *Quart. J. Roy. Meteor. Soc.*, **140**, 595–610, doi:10.1002/qj.2162.

Wieringa, J., 1973: Gust factors over open water and built-up country. *Bound.-Layer Meteor.*, **3**, 424–441, doi:10.1007/BF01034986.

Zappa, G., L. C. Shaffrey, and K. I. Hodges, 2013: The ability of CMIP5 models to simulate North Atlantic extratropical cyclones. *J. Climate*, **26**, 5379–5396, doi:10.1175/JCLI-D-12-00501.1.